

Oligopeptide-strategy of targeting at adipose tissue macrophages using ATS-9R/siCcl2 complex for ameliorating insulin resistance in GDM

Min Wang^{a,b,c,1}, Xuyang Chen^{a,1}, Yanshan Shang^{a,b,c,1}, Bingnan Chen^{a,b,c}, Hao Chen^{a,b,c}, Linwei Zhou^{a,b,c}, Hongli Li^{a,b,c}, Dan Zhang^{a,b,c}, Bailong Tao^d, Xiaobo Zhou^{a,e,*}, Hua Zhang^{a,**}

^a Department of Obstetrics and Gynecology, The First Affiliated Hospital of Chongqing Medical University, Chongqing 400016, China

^b The Chongqing Key Laboratory of Translational Medicine in Major Metabolic Diseases, Chongqing Medical University, Chongqing 400016, China

^c State Key Laboratory of Maternal and Fetal Medicine of Chongqing, Chongqing Medical University, Chongqing 400016, China

^d Department of Rehabilitation Medicine, The First Affiliated Hospital of Chongqing Medical University, Chongqing 400016, China

^e Department of Center for Reproductive Medicine, The First Affiliated Hospital of Chongqing Medical University, Chongqing 400016, China

ARTICLE INFO

Keywords:

CCL2
GDM
Adipose tissue macrophages
Inflammation
Insulin resistance
Targeted gene delivery

ABSTRACT

Gestational diabetes mellitus (GDM) is a pregnancy-specific disease characterized by impaired glucose tolerance during pregnancy. Although diagnosis and clinical management have improved significantly, there are still areas where therapeutic approaches need further improvement. Recent evidence suggests that CCL2, a chemokine involved in immunoregulatory and inflammatory processes, is closely related to GDM. However, the potential value for clinical therapeutic applications and the mechanism of CCL2 in adipose tissue macrophages (ATMs) of GDM remain to be elucidated. Here, we found that CCL2 was enriched in macrophages of the visceral adipose tissue from GDM women and HFD-induced GDM mice. The combination of *in vitro* and *in vivo* experiments showed that *Ccl2* silencing inhibited the inflammatory response of macrophage by blocking calcium transport between ER and mitochondria and reducing excessive ROS generation. Additionally, the ATS-9R/siCcl2 oligopeptide complex targeting adipose tissue was created. Under the delivery of ATS-9R peptide, *Ccl2* siRNA is expressed in ATMs, which reduces inflammation in adipose tissue and, as a result, mitigates insulin resistance. All of these findings point to the possibility that the ATS-9R/siCcl2 complex, which targets adipose tissue, is able to reduce insulin resistance in GDM and the inflammatory response in macrophages. The ATS-9R/siCcl2 oligopeptide complex targeting adipose tissue seems to be a viable treatment for GDM pregnancies.

1. Introduction

Gestational diabetes mellitus (GDM) is defined as glucose intolerance that occurs or is first recognized during pregnancy and affects 4–18 % of pregnant women [1]. GDM can lead to various pregnancy complications, including gestational hypertension and fetal overgrowth, which can result in unfavorable maternal and fetal pregnancy outcomes [2]. Relative insulin deficiency and insulin resistance (IR) are potential pathogenic factors for GDM. Adipose tissue, as one of the peripheral target organs of insulin, plays an essential role in the pathogenesis of GDM [3–5]. In addition, infiltration and activation of adipose tissue macrophages (ATMs) can cause local inflammation and systemic IR, thereby amplifying the inflammatory signaling in adipose tissue. The

activated ATMs secrete a slew of pro-inflammatory cytokines and chemokines such as tumor necrosis factor- α (*TNF- α*), interleukin-6 (*IL-6*), interleukin-1 β (*IL-1 β*), and C-C motif chemokine 2 (*CCL2*), resulting in inflammation throughout the body that inhibits insulin signaling [6–8]. During the onset and development of GDM, numerous macrophages accumulate in visceral adipose tissue (VAT), triggering the release of inflammatory cytokines and mediators [5,6,8]. Therefore, drugs or biologics targeting adipose tissue or ATMs may represent a promising therapeutic option for the treatment of GDM.

CCL2 (also known as monocyte chemoattractant protein-1, MCP-1) is a chemokine for monocytes and a variety of other immune cells. Researchers have shown increasing interest in targeting the CCL2 signaling pathway for potential clinical use in the treatment of cancer,

* Corresponding author at: Department of Obstetrics and Gynecology, The First Affiliated Hospital of Chongqing Medical University, Chongqing 400016, China.

** Corresponding author.

E-mail addresses: xiaobo.zhou@cqmu.edu.cn (X. Zhou), zh2844@gmail.com (H. Zhang).

¹ These authors contributed equally to this work.

Table 1
Gestational characteristics of the study population.

Characteristics	Normal (n=10)	GDM (n=10)	P value
Maternal age (years)	33.33±4.27	33.86±4.12	> 0.05
Gestational age (weeks)	38.83±0.69	39±0.53	> 0.05
BMI (kg/m ²)	26.39±2.81	27.15±3.17	< 0.05
Fasting glucose (mmol/L)	4.43±0.11	5.38±0.25	< 0.05
Glucose after 2 h OGTT (mmol/L)	6.15±0.76	12.01±2.96	< 0.05

BMI - body mass index.

atherosclerosis, multiple sclerosis, and type 2 diabetes [9–12]. CCL2 normally binds to its receptor CCR2, which is primarily expressed in monocytes and promotes cell migration by activating multiple signaling cascades such as JAK2/STAT3, MAPK and PI3K. These signaling pathways ultimately lead to the migration of monocyte into the target tissues [13]. The CCL2/CCR2 pathway is widely known for the recruitment and polarization of macrophages in inflammation. A meta-analysis has shown that CCL2 is a major candidate in the pathogenesis of inflammatory crosstalk in GDM and a potential target for therapeutic intervention [14]. To investigate the physiological role of CCL2 and possible signaling pathways, researchers usually generated *Ccl2* gene knockout mice and injected mice with CCL2 neutralizing antibodies (α CCL2) or CCR2 inhibitors [15,16]. Treatment with α CCL2 reduced glucose tolerance, attenuated inflammation and improved reproductive outcomes in GDM mice [16]. However, injection of CCL2 blockade *in vivo* may act simultaneously on multiple insulin target organs such as liver, muscle and fat, which does not accurately demonstrate that blocking CCL2 in specific tissue or cells would improve systemic symptoms in GDM mice. Therefore, it is necessary to further explore the delivery method of CCL2 and validate its therapeutic target.

Currently, most clinical medications used to treat GDM act downstream of inflammatory processes rather than addressing the underlying causes and may have potential side effects. For example, recent research suggests that low-dose metformin may exacerbate kidney damage [17]. Kim A. Boggess *et al.* reported that the use of metformin plus insulin to treat pre-existing type 2 or gestational diabetes diagnosed early in pregnancy did not result in a reduction in adverse neonatal outcomes [18]. Previous studies have shown that peptide-oligoarginine conjugates (ATS-9R) targeting adipose tissue can effectively transport TNF- α converting enzyme (*Tace*) into the visceral ATMs of mice, reducing adipose tissue inflammation and consequently improving overall metabolism. [19]. As a non-viral gene carrier system, ATS-9R is of great importance for the targeted delivery strategy of gene therapy. In light of this, we hypothesize that encapsulation of *Ccl2* siRNA in ATS-9R could serve as a potential method to inhibit CCL2 in ATMs to ultimately improve overall metabolism in GDM. Here, we show that ATS-9R/siCcl2 complexes effectively accumulate in ATMs by intraperitoneal administration, block calcium transport between ER and mitochondria and reduce excessive ROS production in macrophages, and further inhibit inflammation and IR in GDM mice, making them a potential therapeutic strategy for GDM.

2. Materials and methods

2.1. Clinical sample collection and separation of ATMs

The study was approved by the Ethics Committee of the First Affiliated Hospital of Chongqing Medical University (number: 2020–567). All procedures performed in studies involving human participants were in accordance with the ethical standards of the institutional and/or national research committee and with the 1964 Helsinki Declaration and its later amendments or comparable ethical standards. All gestational diabetes patients and healthy pregnant women were recruited from the First Affiliated Hospital of Chongqing Medical University. Before participation, all individuals had thoroughly read and signed the

Informed Content Document.

Subcutaneous adipose tissue and greater omentum tissue were obtained from 10 normal pregnant women and 10 pregnant women with GDM who had undergone caesarean section at the First Affiliated Hospital of Chongqing Medical University between March 2022 and June 2022. The basic information is shown in Table 1, and the data are expressed as mean \pm standard error. The diagnosis of GDM is based on the results of the 75 g oral glucose tolerance test (OGTT) in pregnant women at 24–28 weeks' gestation. The diagnostic criteria refer to the IADPSG and the international diabetes guidelines: fasting blood glucose \geq 5.1 mmol/L; blood glucose \geq 10.0 mmol/L 1 h after OGTT; blood glucose \geq 8.5 mmol/L 2 h after OGTT. Inclusion criteria: Two groups of pregnant women aged between 20 and 35 years with gestational weeks between 37 and 40 weeks; Both groups of pregnant women conceived naturally; The OGTT results of the normal group are all within the normal range; Two points of elevated blood glucose levels were observed in the OGTT results of the GDM group. Exclusion criteria: hypertension, pre-eclampsia, thyroid disease, renal disease, intrahepatic cholestasis of pregnancy, premature rupture of membranes, premature delivery, twins, infections, and chronic diseases of the immune system.

Subcutaneous adipose tissue and greater omentum tissue were collected and finely minced in cold physiological saline solution. Collagenase was then added at a concentration of 1 mg/ml and incubated at 37 °C for 1 h with shaking. A 70 μ m filter was then used to eliminate adipocytes. After a spin at 400 g for 10 min, the pellet of isolated stromal vascular fraction (SVF) was collected at the bottom. The SVF pellet was resuspended in erythrocyte lysis buffer and incubated for 5 min. To further refine the sample, a 40 μ m filter was used to remove erythrocytes and free leukocytes. The filtered solution was centrifuged at 400 g for 10 min. Subsequently, the SVF pellet was resuspended in 80 μ l MACS buffer and incubated with 20 μ l CD14 microbeads at 4 °C in the dark for 20 min. After washing with MACS buffer, CD14⁺ cells were isolated from the human SVF using the Auto-MACS separator (Miltenyi, Germany) for further assays.

2.2. RNA-seq analysis

The ATMs isolated from the greater omentum of each group were used for total RNA extraction. Libraries were constructed using a TruSeq Stranded mRNA LTSample Prep Kit (Illumina, San Diego, USA) according to the manufacturer's instructions. The generated libraries were analysed using an Agilent 2100 Bioanalyzer (Agilent Technologies, Santa Clara, USA). The libraries were then sequenced on the Illumina sequencing platform (Illumina NovaSeq 6000 PE150). The *P* value < 0.05 and log₂ fold change > 1 was set as the threshold for significantly different expression. GO enrichment and KEGG pathway enrichment of DEGs were performed using the NovoMagic platform (<https://magic.novogene.com>). Upregulated and downregulated genes were separated for analysis.

2.3. Cell culture, siRNA transfection, LPS treatment

RAW264.7 mouse macrophage cells were purchased from ATCC (Virginia, USA) and subcultured every other day in complete medium consisting of Dulbecco's Modified Eagle's Medium (DMEM, Procell Life Technology, Wuhan, China) supplemented with 10 % fetal bovine serum (FBS, Pansera ES, Germany) and 1 % penicillin-streptomycin (Sigma-Aldrich, Saint Louis, MO, United States). Cells were incubated at 37 °C in a humidified atmosphere with 5 % CO₂ and grew to 70–80 % confluence. Then the cells were transfected with Lipofectamine 2000 (Invitrogen, USA) transfection reagent with small interfering RNA (siRNA) for 24 h. The siRNAs were developed and synthesized by GenePharma (Shanghai, China). The detailed information is as follows: Negative control (NC): F: 5-UUCUCCGAACGUGUCACGUTT-3, R: 5-ACGUGACACGUUCGGAGAATT-3; CCL2 siRNA-420, F: 5-GCACCUUUGAAUGUGAAGUTT-3, R: 5-ACUUCACAUCAAAGGUGCTT-3; CCL2 siRNA-259, F: 5-

GUCCCAAAGAAGCUGUAGUTT-3, R: 5-ACUACAGCUUCUUGG-GACTT-3. After transfection, the cells were cultured in the new medium and treated with 100 ng/ml LPS (Biyuntian Biotechnology, Shanghai, China) for 24 h.

2.4. Transmission electron microscopy

RAW264.7 cells were harvested and fixed with 2.5 % glutaraldehyde in 0.2 mol/l phosphate buffer (pH 7.3–7.4) at 4 °C for 2 h. Cells were then postfixed with 1 % osmium tetroxide in 0.2 mol/l phosphate buffer for 2 h. The samples were then dehydrated in a graded ethanol series, infiltrated with propylene oxide, and embedded in Epon. Ultrathin sections were sliced with glass knives on a Leica EM UC7 ultramicrotome, stained with uranyl acetate and lead citrate, and examined with a transmission electron microscope (FEI Tecnai G2 F30; FEI, USA). The contact length between ER and mitochondria was quantified using ImageJ (NIH, Bethesda, MD, USA).

2.5. Mitochondrial stress test

Mitochondrial stress was determined in plated RAW264.7 cells by measuring the oxygen consumption rate with a Seahorse XFe24 Analyzer (Agilent Technology, California, USA). RAW264.7 cells were cultured in 24 well plates with DMEM medium until they reached confluence. Specific groups of cells were transfected with siRNA and treated with LPS. Prior to the assay, the Seahorse XFe24 Extracellular Flux Assay plate was hydrated for 18 h without CO₂ in an XF calibration buffer at 37 °C. Cells were washed with supplemented XF assay medium and equilibrated for 1 h. ATP production, maximal respiration and non-mitochondrial respiration were determined by treating the cells with Oligomycin (1.5 μM), Carbonyl cyanide 4-(trifluoromethoxy) phenylhydrazone (FCCP, 1.0 μM) and Retenone + antimycin A (AA, 0.5 μM), respectively. The oxygen consumption rate was measured using the Wave software (Seahorse Bioscience).

2.6. ATS-9R/siCcl2 complex preparation and in vitro characterization

The adipose tissue targeting sequence (ATS) peptide (CKGGRAKDC) was conjugated with the D-form of 9-arginine (ATS-9R) synthesized by Qiangyao Biotechnology (Shanghai, China). To prepare therapeutic ATS-9R/siCcl2 complexes, the siCcl2 interference fragment was mixed with the ATS-9R carrier and incubated at room temperature (RT) for 30 min. To confirm the condensing effect of the ATS-9R/siCcl2 complexes, the agarose gel retardation assay was performed. After complex formation, the complexes were resolved by electrophoresis on a 0.8 % (w/v) agarose gel at 100 V for 20 min. The surface potential and mean diameter of ATS-9R/siCcl2 complexes were measured using a Zeta Sizer-ZS instrument (Malvern Instruments, Worcestershire, UK). 24 h after cell seeding, the cell culture medium was replaced separately with serum-free medium containing siNC, siCcl2, PEI/siCcl2, and ATS-9R/siCcl2 complexes, after which cell viability was measured by CCK8 assay. After transfection at 0 h, 24 h and 48 h, 100 μl/well cells at the same concentration (3×10^4 cells/ml) were added to the 96-well plate and 10 μl CCK-8 reagent was added to the cell culture medium and incubated for 2 h. An enzyme-labeled instrument was used to detect the optical density (O.D) of the samples at 450 nm (Multiskan Go; Thermo Fisher Scientific).

2.7. GDM mouse model and treatment protocol

The 6-week-old female and male C57BL/6 mice were purchased from Yaokang Biotechnology Co. (Chengdu, China). The study protocols and the use of the animals were approved by the Experimental Animal Administration Committee of Chongqing Medical University. The mice were fed a high-fat diet (HFD, 45 kcal% fat, 35 kcal% carbohydrate, 20 kcal% protein) to induce a GDM model. After a 1-week normal chow

diet, the female mice were divided into two groups: Control and HFD, then they were mated separately with male mice. On the next day, the plugged-mated females were designated as gestation day (GD) 0.5. While the control group continued to receive normal chow, the HFD group was fed high-fat chow (D12451, Research Diets) until GD 17.5. Two independent animal experiments were performed and a representative result was shown.

In the subsequent drug intervention experiments, HFD-induced GDM mice were divided into a control group (PBS 0.1 ml/10 g) and a drug injection group (Fendiline 6.8 μg/kg, MitoQ 6.8 μg/kg, ATS-9R/NC 0.35 mg/kg and ATS-9R/siCcl2 0.35 mg/kg). From GD 13.5, the intraperitoneal injection was administered every day, four times during the trial period. On GD 17.5, subcutaneous adipose tissue and visceral adipose tissue were harvested to obtain SVFs for subsequent experiments, using the same method as for obtaining human SVFs.

2.8. Oral Glucose Tolerance Test (OGTT) and insulin tolerance test (ITT)

Initial blood glucose levels were measured after 6 h of fasting using an Accu-Chek Active model GC kit (Roche Diagnostics GmbH) in 5–6 mice per group. After checking baseline blood glucose levels, insulin (0.75 U/kg) was injected intraperitoneally or glucose (2 g/kg) was ingested orally. Blood samples were taken from the tail vein at 0, 15, 30, 60, 90 and 120 min after drug administration.

2.9. Mouse bone marrow-derived macrophage cultures

Under sterile conditions, bone marrow-derived macrophages (BMDMs) were isolated from the femur and tibia of 6–8-week-old mice and cultured for 7 days in RPMI medium containing 10 % FBS (Pansera ES, Germany), 100 U/ml penicillin-streptomycin, 200 mM glutamine (Sigma-Aldrich, Saint Louis, MO, United States) and 10 ng/l macrophage colony-stimulating hormone (M-CSF; Novoprotein, Suzhou, China).

2.10. Biodistribution

Cy5.5 was conjugated to ATS-9R carriers by Qiangyao Biotechnology (Shanghai, China) and the siCcl2 interference fragment was incubated with Cy5.5-ATS-9R for 30 min at RT. Subsequently, the Cy5.5-conjugated complexes were injected intraperitoneally into pregnant mice at GD 16.5 (gene dose: 0.2 mg/kg). 8 h and 24 h after injection, the mice were sacrificed and the visceral adipose tissue, subcutaneous adipose tissue, liver, spleen, heart, lung, kidney, and placenta were harvested for ex vivo analysis. The total fluorescence in each organ was visualized using an Image Station (IndiGo) instrument.

2.11. Blood chemistry analysis

After isoflurane anesthesia in mice, whole blood and serum were collected. The concentrations of liver enzymes (aspartate aminotransferase (AST) and alanine aminotransferase (ALT)) and renal function (blood urea nitrogen (BUN)) were measured in the control and treatment groups. Blood cell counts including white blood cells (WBC), red blood cells (RBC) and hemoglobin (HGB) were measured by whole blood analysis. All measurements were performed using the Catalyst One (IDEXX, USA) and an automated hematology analyzer (SYSMEX, Japan).

2.12. Enzyme-linked immunosorbent assay (ELISA)

ELISA was performed to determine the concentration of TNF-α, IL-6, IL-1β and CCL2 in the supernatant of RAW264.7 cells and in the serum of mice. The commercially available TNF-α, IL-6, IL-1β and CCL2 ELISA kits for mice (AB-2868A, AB-5737A, AB-2776A and AB-W30368 Abmart Shanghai Co., Ltd., China) were used according to the manufacturer's

instructions. Use of the mouse p-AKT ELISA kit (Cat. # RX203621M RUIXIN BIOTECH, China) allowed for the detection of p-AKT levels in the liver and muscle of the mice according to the manufacturer's instructions.

2.13. Immunofluorescence staining

RAW264.7 cells were fixed in 4 % paraformaldehyde (PFA) for about 20 min. After washing three times with PBS, the cells were permeabilized with 0.5 % Triton X-100 for 20 min at room temperature, washed three times with PBS, and then blocked in 5 % bovine serum albumin (BSA) (Sangon Biotech, Shanghai, China) for 30 min. The primary antibody against Prohibitin (Abcam, Cambridge, UK) was incubated with the samples overnight at 4 °C. After washing three times with PBS, the samples were incubated with donkey anti-rabbit IgG H&L (Alexa Fluor® 488) (Abcam, Cambridge, UK) as a secondary antibody for 1 h at room temperature. Finally, cells were washed three times, incubated with Hoechst-33342 (Solarbio, Beijing, China) and CellMask™ plasma membrane dye (Thermo Fisher Scientific, Waltham, MA, USA) for 10 min, and mounted in glycerol solution. Confocal images were captured using the Zeiss LSM800 system (Carl Zeiss, Oberkochen, Germany) and processed using Adobe Photoshop software (Adobe, San Jose, CA, USA). A similar staining procedure was used for BMDM cells.

RAW264.7 cells and BMDM cells were fixed in 4 % PFA after incubation with Cy5.5-ATS-9R (5 µg/ml) and Cy5.5-ATS-9R/siCcl2 (5 µg/l), respectively. After washing three times with PBS, the cells were permeabilized with 0.5 % Triton X-100 for 20 min at room temperature, washed three times with PBS and then blocked with 5 % BSA. The cells were then washed three times, incubated with Hoechst-33342 and DiO (Cell Membrane Green Fluorescence Probe) (Beyotime, Shanghai, China) for 10 min, and mounted in glycerol solution. The Zeiss LSM800 system was used to obtain confocal images. The Living Cell Workstation (OLYMPUS IX83, Japan) records the process of internalization of Cy5.5-ATS-9R by RAW264.7 cells.

Intracellular calcium levels were determined using the calcium-sensitive indicator Calbryte 520 (AAT Bioquest, USA) according to the manufacturer's instructions. In brief, cells were loaded after treatment with 10 µM Calbryte 520, 5 µM ER-Tracker (Thermo Fisher Scientific, Waltham, MA, USA) and 0.02 % (W/V) Pluronic F-127 (Beyotime, Shanghai, China) for 20 min at 37 °C in the absence of light. Cells were gently washed three times with HBSS (Hanks' balanced salt solution) buffer and then incubated with Hoechst-33342 for 10 min before imaging with a fluorescence microscope. For mitochondrial calcium level measurement, RAW264.7 cells were loaded with 5 µM Rhod-2 AM (Thermo Fisher Scientific, Waltham, MA, USA), 10 µM MitoTracker (Thermo Fisher Scientific, Waltham, MA, USA) and 0.02 % Pluronic F-127 for 30 min at room temperature. Prior to fluorescence measurement, cells were washed and incubated for 30 min to ensure complete de-esterification of mitochondrial AM esters, followed by an additional incubation with Hoechst-33342 for 10 min.

Intracellular ROS generation was measured using 2',7'-dichlorofluorescein diacetate (DCFH-DA, Thermo Fisher Scientific, Waltham, MA, USA), a cell-permeable ROS indicator. Cells were pre-incubated with 10 µM DCFH-DA for 20 min at 37 °C, then ROS-mediated fluorescence was observed under a confocal microscope. Mitochondrial superoxide is generated as a by-product of oxidative phosphorylation. The mitochondrial superoxide indicator MitoSOX Red (Thermo Fisher Scientific, Waltham, MA, USA) is a novel fluorogenic dye for the highly selective detection of superoxide in the mitochondria of living cells. Cells were pre-incubated with 5 µM MitoSOX Red for 15 min at 37 °C and then incubated with Hoechst-33342 for 10 min at RT. A similar staining procedure was used for adipose tissue. Fluorescence mediated by mitochondrial ROS was observed in real-time under a confocal microscope.

2.14. Flow cytometry

SVF cells isolated from human adipose tissue were incubated for 15 min at room temperature with 100 µl live/dead dye PE-Texas Red (Biolegend, Beijing, China) before staining for 30 min at 4 °C with CD45-APC-Cy7, CD14-FITC, CD86-PE (Biolegend, Beijing, China). After washing the cells twice with PBS, 100 µl Fix/Perm buffer was added to resuspend the sediment and then incubated at room temperature for 30 min. The cells were centrifuged at 400 g for 5 min and the supernatant was discarded. CD206-APC antibody (Biolegend, Beijing, China) was then added to the cell suspension and incubated for 30 min, followed by two washes in PBS.

SVF cells isolated from mouse adipose tissue were incubated for 15 min at room temperature with 100 µl live/dead dye PE-Texas Red, followed by staining with CD45-DAPI, CD11b-PerCP-Cy5.5, F4/80-APC, CD86-PE (Biolegend, Beijing, China) for 30 min at 4 °C. After washing twice with PBS, 100 µl Fix/Perm buffer was used to resuspend the sediment and incubated for 30 min at room temperature. Cells were then resuspended in 500 µl 1x perm wash buffer cells and centrifuged at 400 g for 5 min. Then CD206-FITC (Biolegend, Beijing, China) was added to the suspension and incubated for 30 min, followed by two washes in PBS. A similar staining procedure was applied to RAW264.7 cells. Macrophage polarization was then determined by BD FACScan flow cytometry.

Flow cytometry was used to quantify the expression levels of calcium ions and ROS in mouse ATMs. In brief, SVF cells were stained with CD45, CD11b, F4/80, and 5 µM Calbryte 520 for 30 min at room temperature in the dark. Similarly, 5 µM Rhod-2 AM was used to measure mitochondrial calcium levels, while intracellular ROS generation was measured with 5 µM H2DCFDA and 5 µM MitoSOX Red was applied to indicate mitochondrial superoxide levels. A similar staining procedure was performed for RAW264.7 cells. Data acquisition and analysis was performed using a BD FACScan flow cytometer and FlowJo software (TreeStar, CA, USA).

2.15. Quantitative reverse transcription-polymerase chain reaction (qRT-PCR)

Trizol reagents (Sigma-Aldrich, Saint Louis, MO, United States) were used to extract total RNA. Evo M-MLV RT Mix Kit (Accurate Biology, Changsha, China) was then used for reverse transcription. The Bio-Rad CFX96 Real-Time PCR System (Bio-Rad Laboratories, Hercules, CA, USA) was used to perform qRT-PCR with the SYBR Green Premix Pro Taq HS qPCR Kit (Accurate Biology, Changsha, China), and 2^{-ΔΔCt} method (Ct values are threshold cycles) was performed to calculate relative mRNA levels. All samples were normalized with glyceraldehyde-3-phosphate dehydrogenase (GAPDH), which was used as an internal reference gene. Experiments were repeated independently for at least three times. The primers used in the qRT-PCR assay are listed in [Supplementary Table S1](#).

2.16. Statistical analysis

Cell counting, distance measurement, and fluorescence intensity were performed using Image J software (imagej.nih.gov/ij). Experiments were repeated at least three times. Quantitative data are presented as mean ± standard error of the mean (SEM). Data were analysed for statistical differences using Student's t-test and one-way ANOVA by GraphPad software (La Jolla, CA, USA). *P* value < 0.05 was considered an indicator of statistical significance.

3. Results

3.1. Pregnancies with GDM exhibit higher CCL2 level in ATMs

Adipose tissue, particularly white visceral adipose tissue, is a key target organ for insulin activity and is considered an important site for

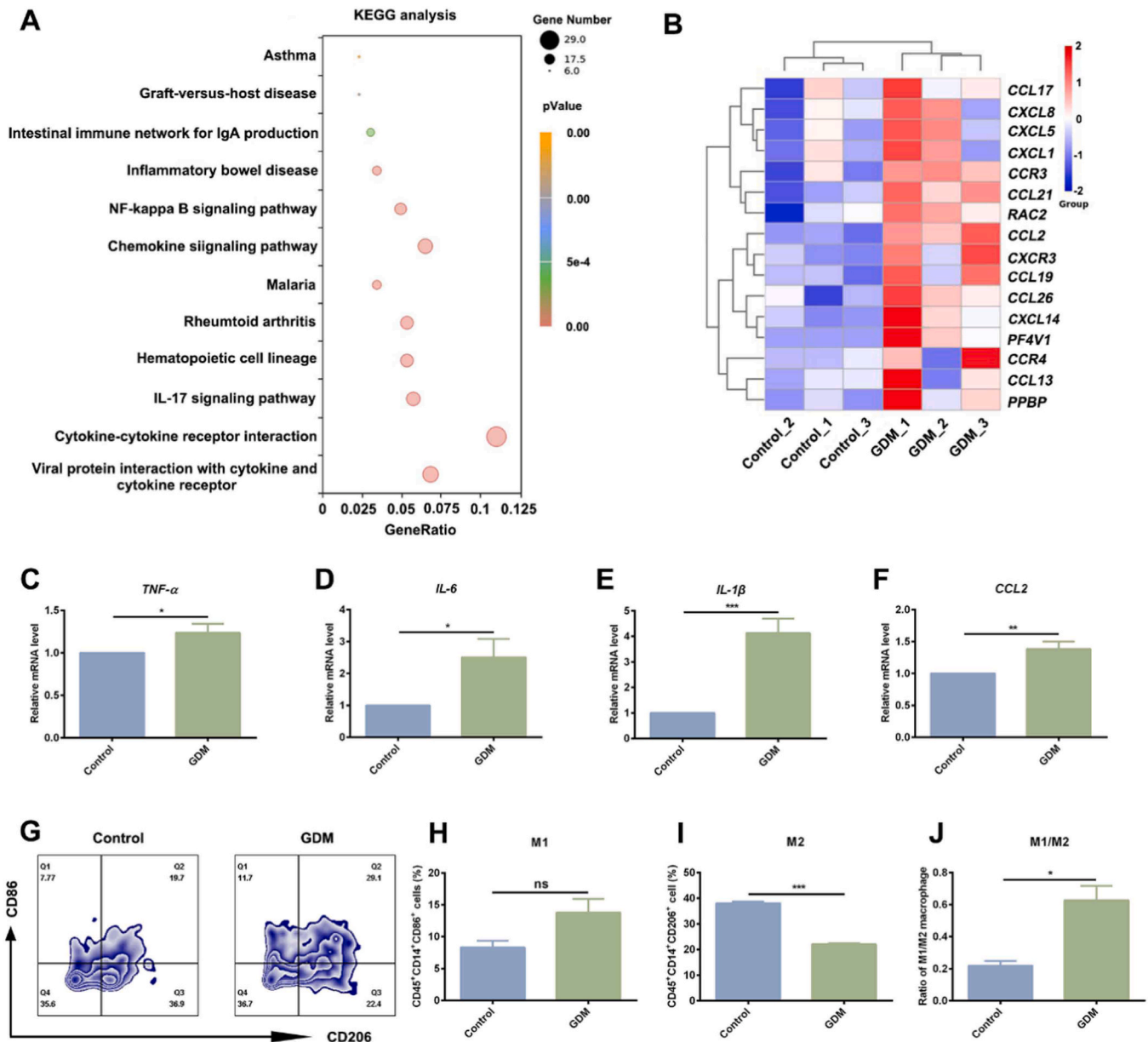


Fig. 1. Higher CCL2 expression is associated with pro-inflammatory ATMs in GDM pregnancies. **A.** KEGG enrichment analysis showed that the differentially expressed genes were associated with the chemokine signaling pathway in GDM pregnancies. **B.** Heatmap showing the differential expression of genes associated with chemokine signaling pathway. **C-F.** qRT-PCR analysis of *TNF-α*, *IL-6*, *IL-1β* and *CCL2* in ATMs from normal and GDM pregnancies (n = 3). **G.** Flow cytometric analysis of M1-type and M2-type macrophages in SVFs (n = 3). **H.** Percentage of CD45⁺CD14⁺CD86⁺ cells in SVFs (n = 3). **I.** Percentage of CD45⁺CD14⁺CD206⁺ cells in SVFs (n = 3). **J.** The ratio of CD45⁺CD14⁺CD86⁺ cells to CD45⁺CD14⁺CD206⁺ cells (n = 3). **P* < 0.05, ***P* < 0.01, ****P* < 0.001, ns represents no significance.

inflammation. To determine the degree of inflammation between GDM and normal pregnancies, we collected adipose tissue. Consistent with previous findings, our results showed a specific increase in inflammatory genes such as *TNF-α*, *IL-6* and *IL-1β* in VAT of GDM pregnancies (Fig. S1). Since macrophages contribute significantly to adipose tissue inflammation, we extracted SVFs from the greater omentum and then isolated CD14⁺ macrophages using magnetic beads. Whole-transcriptome RNA sequencing (RNA-seq) of ATMs between control and GDM pregnancy was then performed. 407 upregulated genes and 198 downregulated genes were identified in ATMs (Fig. S2: Log₂(fold change) > 1, *P* value < 0.05). To further investigate the signaling pathways affected by GDM, an analysis of the Kyoto Encyclopedia of Genes and Genomes (KEGG) was performed. Interestingly, KEGG analysis revealed enrichment of differential genes in the chemokine signaling pathway (Fig. 1A), with

heatmap analysis showing significantly upregulated expression of CCL2 in ATMs from GDM pregnancies (Fig. 1B). In addition, qRT-PCR results confirmed the increased expression of pro-inflammatory factors in ATMs from GDM pregnancies, including *TNF-α*, *IL-6*, *IL-1β* and *CCL2* (Fig. 1C-F). During obesity, ATMs tend to polarize toward the pro-inflammatory M1 phenotype, which promotes adipose tissue inflammation and systemic IR. As shown in Fig. 1G-J, flow cytometry analysis indicates a shift toward the pro-inflammatory M1 phenotype in ATMs from the GDM pregnancies.

Next, we used HFD to induce the GDM mouse model. As shown in Fig. S3, the HFD-induced GDM mice exhibited persistently high blood glucose levels from mid to late gestation, accompanied by significant IR and fetal weight gain in late gestation, reflecting the characteristics of human GDM. In addition, ATMs from VAT in HFD-induced GDM mice

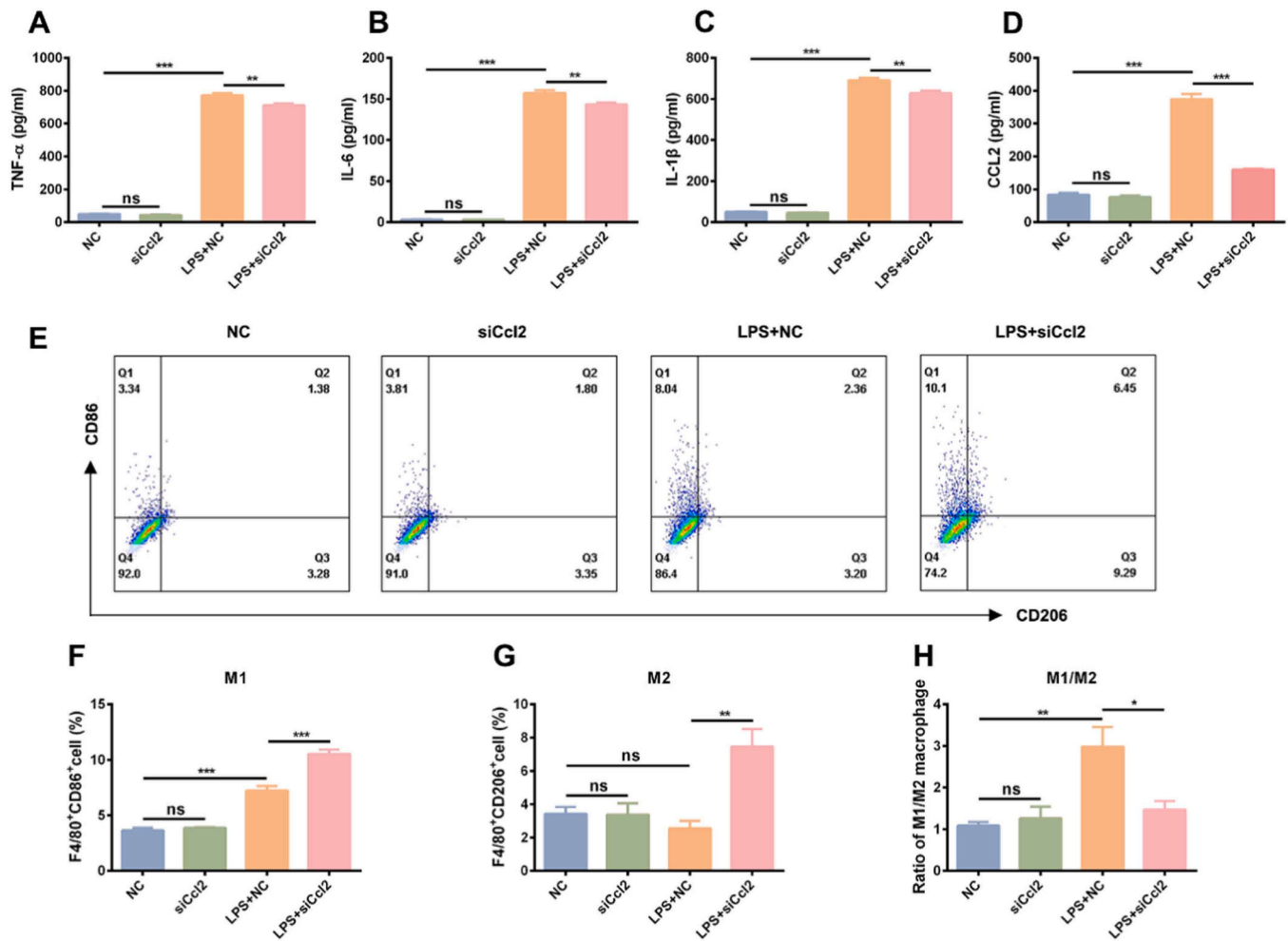


Fig. 2. Silencing *Ccl2* inhibits pro-inflammatory polarization of LPS-stimulated RAW264.7 cells. A-D. The levels of TNF- α , IL-6, IL-1 β and CCL2 in cell culture medium harvested from NC, siCcl2, LPS + NC and LPS + siCcl2-treated RAW264.7 cells, as determined by ELISA (n = 3). E. Flow cytometric analysis of the percentage of M1-type and M2-type macrophages (n = 3). F. Percentage of F4/80⁺CD86⁺ cells (n = 3). G. Percentage of F4/80⁺CD206⁺ cells (n = 3). H. Ratio of F4/80⁺CD86⁺ cells to F4/80⁺CD206⁺ cells (n = 3). **P* < 0.05, ***P* < 0.01, ****P* < 0.001, ns represents no significance.

exhibited elevated levels of pro-inflammatory factors (*Tnf- α* , *Il-6*, *Il-1 β* and *Ccl2*) and M1/M2 macrophage ratio increased, indicating a pronounced inflammatory response of macrophages in VAT (Fig. S4). Taken together, these findings show an enhanced inflammatory response in macrophages as well as higher CCL2 levels in ATMs from both GDM pregnancies and HFD-induced GDM mice.

3.2. *CCL2* exhibits potential therapeutic target

Previous studies suggested that blocking CCL2 could be a promising strategy for the treatment of GDM [16]. Considering the significant increase of CCL2 in ATMs, we want to test how silencing *Ccl2* affects the regulation of inflammatory response. To this end, the interference efficiency of two siRNAs (*Ccl2* siRNA-420 and *Ccl2* siRNA-259) was evaluated and *Ccl2* siRNA-259 was selected for subsequent experiments in RAW264.7 cells (Fig. S5). Then, lipopolysaccharide (LPS) was used to induce a macrophage inflammation model in vitro. As shown in Fig. 2A-D, knocking down *Ccl2* led to a decrease in pro-inflammatory factors (*Tnf- α* , *Il-6*, *Il-1 β* and *Ccl2*) in LPS-stimulated RAW264.7 cells. Furthermore, we detected the change in macrophage polarization upon *Ccl2* loss by flow cytometry. Our analysis revealed a decreased ratio of M1/M2 macrophages in the LPS-induced and siCcl2-treated groups (Fig. 2E-H). These results indicate that loss of *Ccl2* attenuates the inflammatory response in LPS-stimulated RAW264.7 cells, suggesting that targeting CCL2 may be a potential therapeutic target.

3.3. *CCL2* controls calcium transfer, ROS, and mitochondrial function in polarized macrophages

Gene Ontology (GO) analysis of differential DEGs in ATMs was performed and revealed alterations in the regulation of calcium ion homeostasis, calcium ion concentration, and calcium ion transport between GDM and normal pregnancies (Fig. S6). Interestingly, CCL2 is one of the upregulated genes associated with calcium ion transport in ATMs from GDM pregnancies (Fig. 3A).

Previous studies have demonstrated the close coordination between Ca²⁺ release in the ER and mitochondrial Ca²⁺ uptake in regulating numerous aspects of mitochondrial biology and function [20]. Here, we used Calbryte 520 and ER-Tracker to display ER Ca²⁺, and found a decreased level of ER Ca²⁺ in LPS-induced RAW264.7 cells when *Ccl2* was knocked down (Fig. 3B and C). Furthermore, the level of mitochondrial Ca²⁺ was determined by Rhod-2 AM (an indicator of mitochondrial calcium), which overlapped with the mitochondrial marker Mito-Tracker, and decreased dramatically in the LPS-induced and siCcl2-treated RAW264.7 cells (Fig. 3D and E). Similar results were also verified by flow cytometry (Fig. S7A-D). The contact sites where the ER communicates with the mitochondria are referred to as mitochondria-associated ER membranes (MAMs) [21]. It was found that LPS stimulation resulted in alteration of macrophage ultrastructure as evidenced by ER rupture and vacuolization, mitochondrial pyknosis and rupture of mitochondrial cristae in transmission electron microscopy.

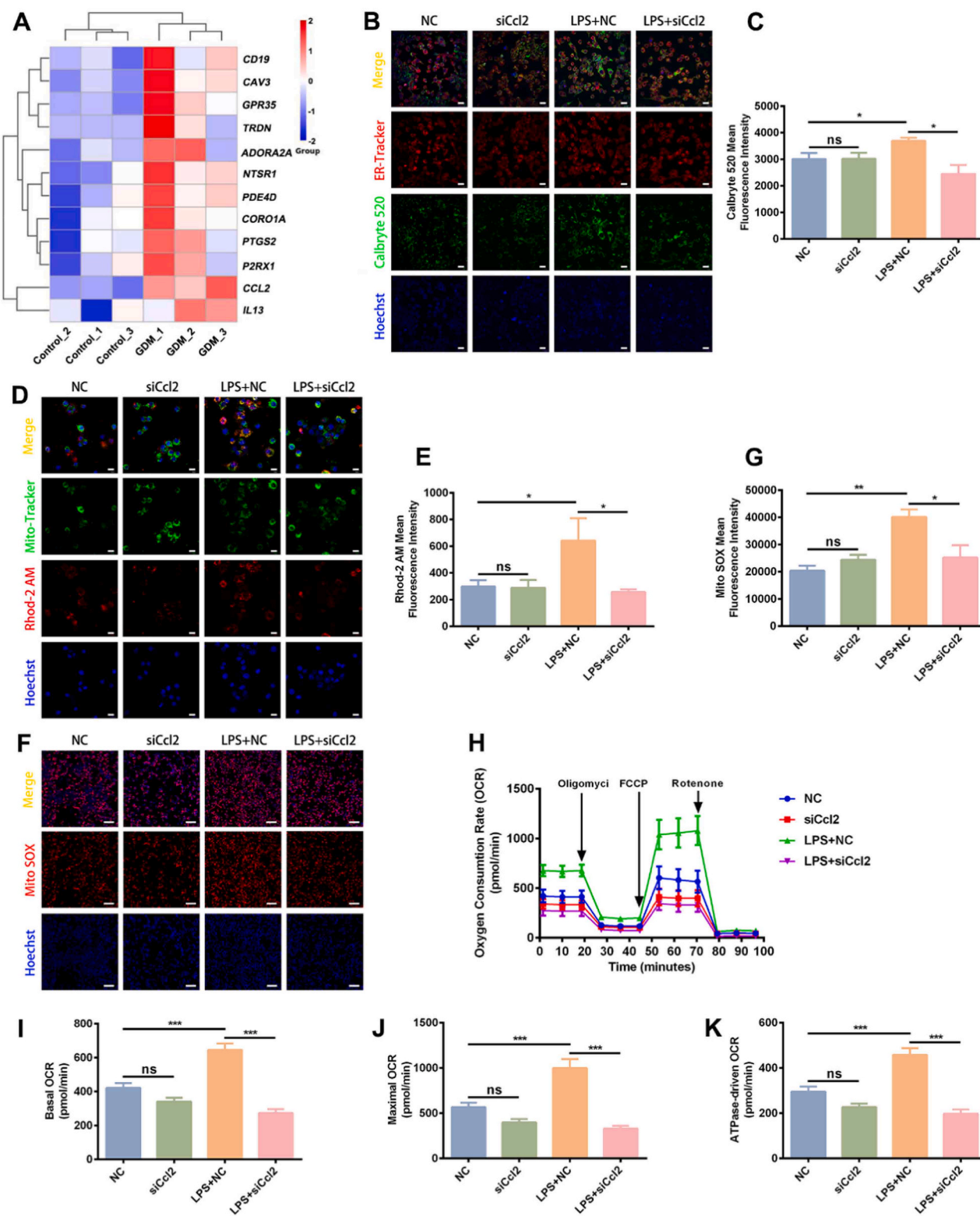


Fig. 3. Inhibiting *Ccl2* blocks ER-mitochondria calcium transport, reduces ROS production and improves mitochondrial function in LPS-induced RAW264.7. **A.** Heatmap showing differentially expressed genes in the regulation of Ca^{2+} transport in ATMs from GDM and normal pregnancies. **B.** Representative confocal microscopy images of fluorescence staining for ER-Tracker (red), Calbryte 520 (green), and Hoechst (blue) in NC, siCcl2, LPS + NC, and LPS + siCcl2-treated RAW264.7 cells. Scale bar = 20 μ m. **C.** Quantification of Calbryte 520 fluorescence intensity in (B) (n = 5). **D.** Representative confocal microscopy images of fluorescence staining for Mito-Tracker (green), Rhod-2 AM (red), and Hoechst (blue). Scale bar = 20 μ m. **E.** Quantification of Rhod-2 AM fluorescence intensity in (D) (n = 5). **F.** Confocal microscopy detection of ROS in RAW264.7 cells stained with Mito Sox (red). Scale bar = 75 μ m. **G.** Quantification of Mito Sox fluorescence intensity in (F) (n = 4). **H.** Analysis of oxygen consumption rate (OCR) by Seahorse assay (n = 3). **I.** Oligomycin inhibits ATP synthesis. **J.** FCCP uncouples oxygen consumption from ATP production. **K.** AA + Rotenone inhibits complexes I and III. **P* < 0.05, ***P* < 0.01, ****P* < 0.001, ns represents no significance.

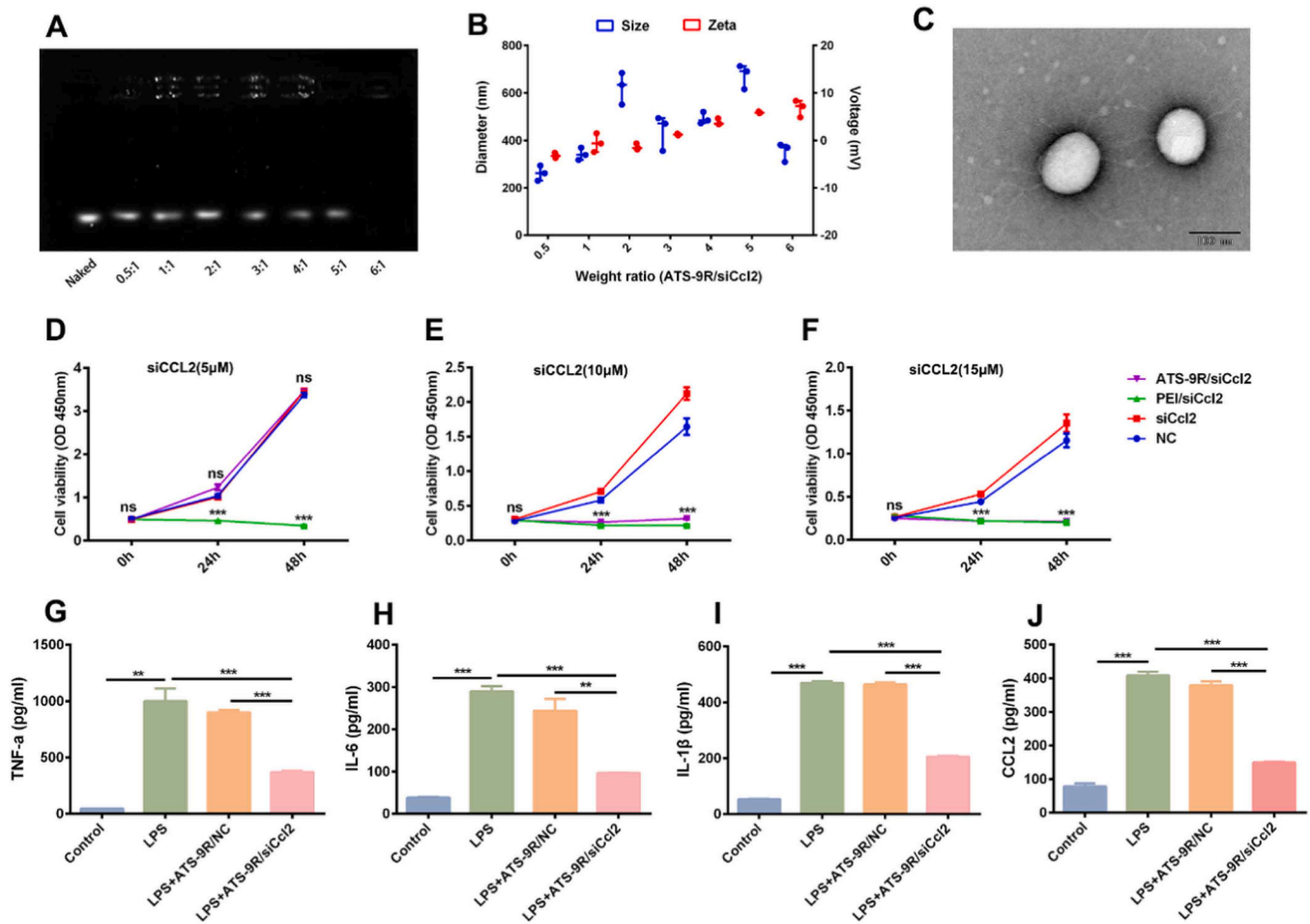


Fig. 4. Characterization of ATS-9R/siCcl2 complexes and biological functions on inflammatory response in LPS-induced RAW264.7 cells. **A.** Gene retardation assay of ATS-9R/siCcl2 complexes. **B.** DLS analysis of ATS-9R/siCcl2 complexes ($n = 3$). **C.** TEM image of ATS-9R/siCcl2 complexes. Scale bars = 100 nm. **D-F.** The effect of ATS-9R/siCcl2 complexes on cell viability was determined by CCK8 assay ($n = 3$). **G-J.** The levels of TNF- α , IL-6, IL-1 β and CCL2 in cell culture medium harvested from blank, LPS, LPS + ATS-9R/NC, and LPS + ATS-9R/siCcl2-treated cells, as analyzed by ELISA ($n = 3$). ** $P < 0.01$, *** $P < 0.001$, ns represents no significance.

However, in the LPS-induced and siCcl2-treated group, only partial mild rupture of the mitochondria was observed (Fig. S8A). The mean distance between the ER and the outer mitochondrial membrane (OMM) was larger in the LPS-induced and siCcl2-treated RAW264.7 cells, suggesting that reduced calcium transfer from the ER to the mitochondria may result in less mitochondrial calcium overload (Fig. S8B).

Excessive and/or sustained Ca^{2+} influx would lead to increased mitochondrial ROS (mROS) production [22]. In this study, ROS level was measured by H2DCFDA and Mito Sox staining, and we found that Ccl2 silencing decreased LPS-induced intracellular and mitochondrial ROS production (Fig. S9). Similar results were confirmed by flow cytometry (Fig. S7E-H). Given the significant effects of mitochondrial oxidative stress on mitochondrial function, we also demonstrated that downregulation of Ccl2 improved the LPS-induced increase in basal respiration (before oligomycin), maximum respiratory capacity (after FCCP), and ATPase-driven respiration (Δ OCR [oxygen consumption rate] basal-oligo) (Fig. 3H-K), suggesting that Ccl2 silencing attenuates inflammation-induced mitochondrial dysfunction. In addition, genes involved in the mitochondrial respiratory chain (MRC), including cytochrome c oxidase (COX), ATP synthase, and NADH: ubiquinone oxidoreductase family (NDUFs), were significantly downregulated after knockdown of Ccl2 in LPS-stimulated RAW264.7 cells (Fig. S10). Taken together, these data suggest that knockdown of Ccl2 attenuates calcium transfer from the ER to mitochondria, reduces intracellular and mitochondrial ROS accumulation, and improves mitochondrial function in

LPS-stimulated RAW264.7 cells.

In vivo, increased levels of intracellular and mitochondrial Ca^{2+} and ROS were observed in ATMs from GDM mice (Fig. S11). Next, the calcium channel blocker Fendiline and the mitochondrial antioxidant MitoQ were used to further demonstrate whether CCL2 blocks calcium transport between ER and mitochondria and reduces excessive ROS production, thereby regulating inflammatory responses in macrophages. In ATMs from GDM mice with Fendiline treatment, we found a significant decrease in mRNA levels of *Tnf- α* , *Il-1 β* and *Ccl2* (Fig. S12A and B). In addition, mRNA expression of *Tnf- α* , *Il-6*, *Il-1 β* and *Ccl2* was downregulated in ATMs from GDM mice by treatment with MitoQ (Fig. S12C and D). Flow cytometric analysis also showed a decrease in the ratio of M1/M2 macrophages, indicating a reduction in the inflammatory response in ATMs (Fig. S13). Moreover, the levels of intracellular and mitochondrial Ca^{2+} and ROS were decreased in ATMs from GDM mice by treatment with Fendiline or MitoQ (Fig. S14). Finally, Fendiline and MitoQ effectively improved insulin sensitivity (Fig. S15) and reproductive outcomes (Fig. S16) in GDM mice. Accordingly, in LPS-induced RAW264.7 cells, we demonstrated that Fendiline and MitoQ inhibited the inflammatory response (Fig. S17 and S18) and downregulated the levels of intracellular and mitochondrial Ca^{2+} and ROS (Fig. S19). These observations suggest that CCL2 mediates calcium transfer and ROS generation to regulate macrophage polarization.

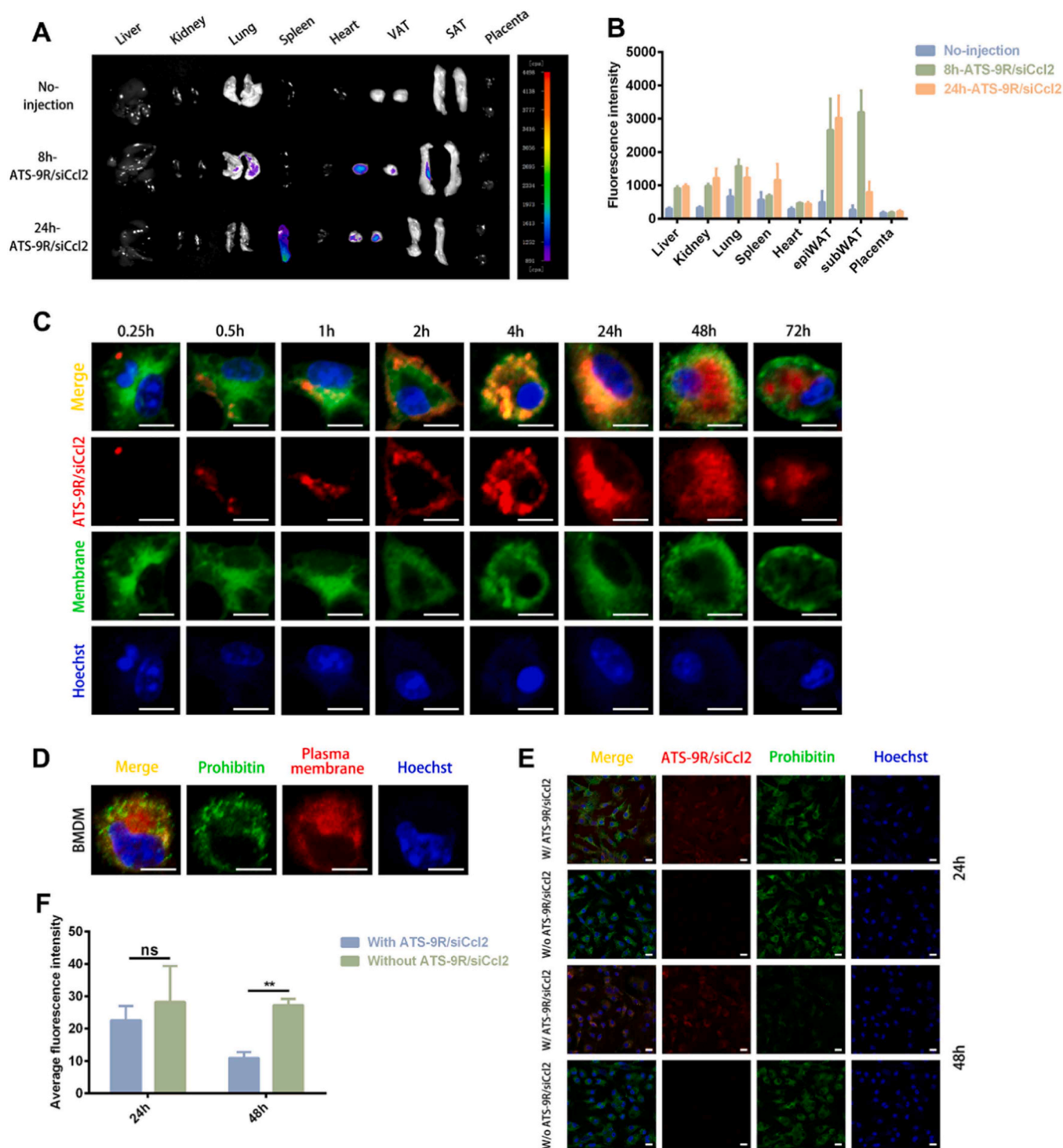


Fig. 5. BMDM cells internalize ATS-9R/siCcl2 complexes through prohibitin protein. A. Biodistribution image of Cy5.5-ATS-9R/siCcl2 at 8 h and 24 h post intraperitoneal injection. B. Total fluorescence intensity in various organs (n = 3). C. Time-dependent intracellular localization of Cy5.5-ATS-9R/siCcl2 in BMDM cells. Scale bar = 100 μ m. D. Immunostaining of prohibitin (green), Plasma membranes (Cellmask Deep Red), and Hoechst (blue) in BMDM cells. Scale bar = 100 μ m. E. Immunostaining of prohibitin in BMDM cells treated with or without Cy5.5-ATS-9R/siCcl2 (red) (n = 4). Scale bar = 20 μ m. F. Average fluorescence intensity of prohibitin in (E). ** $P < 0.01$, ns represents no significance.

3.4. ATS-9R/siCcl2 complexes specifically target adipose tissue and are internalized by macrophages

Considering that ATS-9R can efficiently target adipose tissue, we sought to combine ATS-9R with *Ccl2* siRNA fragments and then validate the function of the synthesized ATS-9R/siCcl2 complexes in regulating the inflammatory response in macrophages. The characterization of the

ATS-9R/siCcl2 complexes was first verified *in vitro*. The agarose gel retardation experiment showed that the ATS-9R-complexed siCcl2 is retarded at a weight ratio of 6 (Fig. 4A). The ATS-9R/siCcl2 complexes had a diameter of about 354 nm and a charge of 7 mV at a weight ratio of 6 (Fig. 4B). The representative TEM image of the ATS-9R/siCcl2 complexes is shown in Fig. 4C. CCK8 assay showed that there was no effect on cell survival ability when the mass ratio of ATS-9R/siCcl2 was

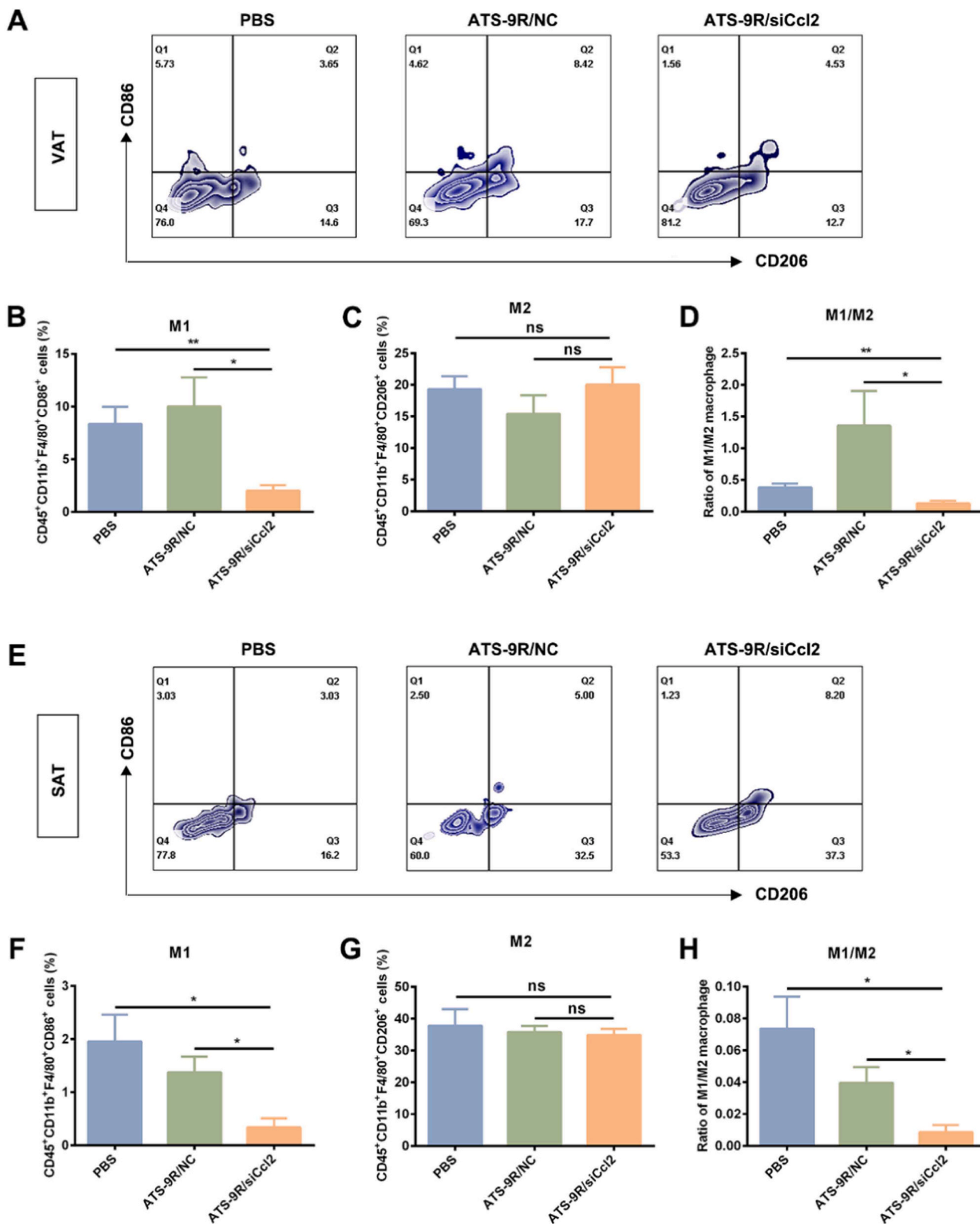


Fig. 6. AT5-9R/siCcl2 complexes attenuate pro-inflammatory polarization of ATMs in GDM mice. A. Flow cytometric analysis of M1-type and M2-type macrophages in SVFs isolated from VAT. B. Percentage of CD45⁺CD11b⁺F4/80⁺CD86⁺ cells in VAT (n = 6–8). C. Percentage of CD45⁺CD11b⁺F4/80⁺CD206⁺ cells in VAT (n = 6–8). D. Ratio of CD45⁺CD11b⁺F4/80⁺CD86⁺ cells to CD45⁺CD11b⁺F4/80⁺CD206⁺ cells in VAT (n = 6–8). E. Flow cytometric analysis of M1-type and M2-type macrophages in SVFs isolated from SAT. F. Percentage of CD45⁺CD11b⁺F4/80⁺CD86⁺ cells in SAT (n = 6–8). G. Percentage of CD45⁺CD11b⁺F4/80⁺CD206⁺ cells in SAT (n = 6–8). H. Ratio of CD45⁺CD11b⁺F4/80⁺CD86⁺ cells to CD45⁺CD11b⁺F4/80⁺CD206⁺ cells in SAT (n = 6–8). *P < 0.05, **P < 0.01, ns represents no significance.

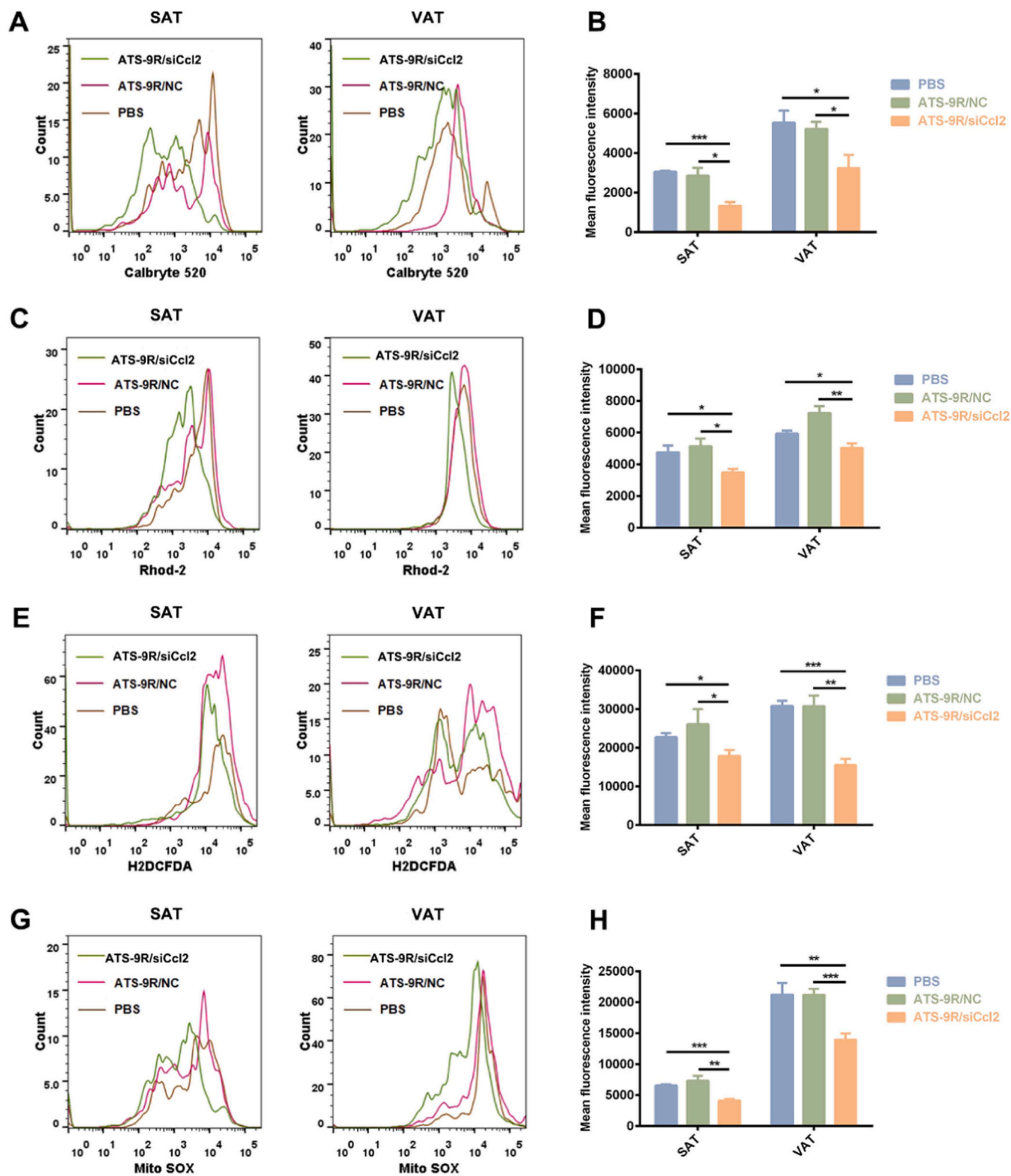


Fig. 7. ATS-9R/siCcl2 complexes block ER–mitochondria Ca²⁺ transport and reduce ROS production in ATMs of GDM mice. A-B. Flow cytometric analysis of Calbryte 520 in CD45⁺CD11b⁺F4/80⁺ cells from SVFs. Quantification of mean fluorescence intensity (n = 4–6). C-D. Flow cytometry analysis of Rhod-2 in CD45⁺CD11b⁺F4/80⁺ cells from SVFs. Quantification of mean fluorescence intensity (n = 4–6). E-F. Flow cytometric analysis of H2DCFDA in CD45⁺CD11b⁺F4/80⁺ cells from SVFs. Quantification of mean fluorescence intensity (n = 4–6). G-H. Flow cytometry analysis of Mito SOX in CD45⁺CD11b⁺F4/80⁺ cells from SVFs. Quantification of mean fluorescence intensity (n = 4–6). *P < 0.05, **P < 0.01, ***P < 0.001.

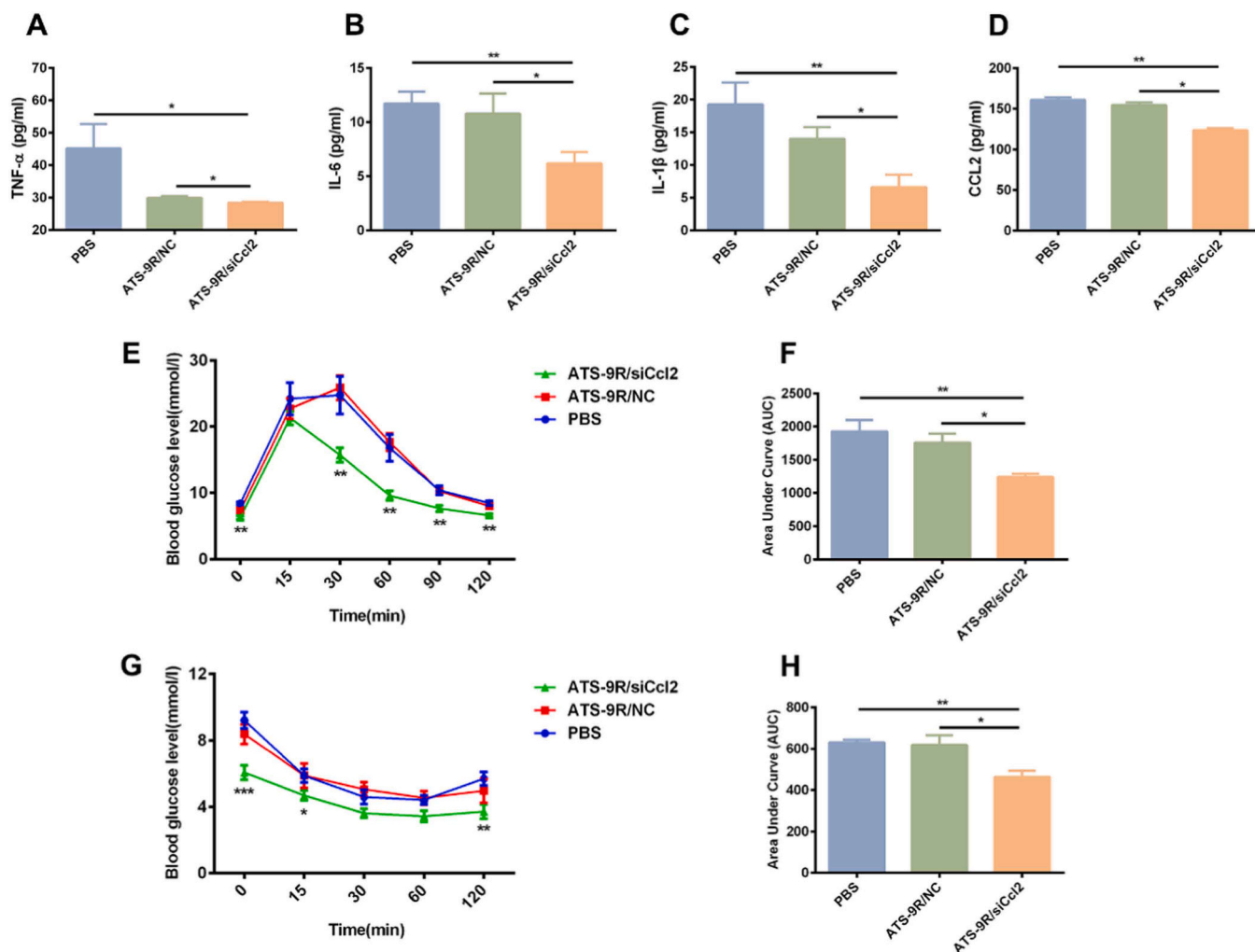


Fig. 8. ATS-9R/siCcl2 complexes reduce blood cytokine levels and enhance insulin sensitivity in GDM mice. A-D. The levels of TNF- α (n = 5–6), IL-6 (n = 6–10), IL-1 β (n = 9–10) and CCL2 (n = 4–6) in the serum from GDM mice treated with PBS, ATS-9R/NC, or ATS-9R/siCcl2, as analyzed by ELISA. E-F. Glucose tolerance tests in GDM mice treated with PBS, ATS-9R/NC, or ATS-9R/siCcl2. The areas under the curves were integrated from the various graphs and compared (n = 4–6). G-H. Insulin tolerance test in GDM mice treated with PBS, ATS-9R/NC, or ATS-9R/siCcl2. The areas under the curves were integrated from the various graphs and compared (n = 4–6). * $P < 0.05$, ** $P < 0.01$, *** $P < 0.001$.

6 at a concentration of 5 μ M siCcl2 (Fig. 4D-F). We then administered ATS-9R-complexed siCcl2 into RAW264.7 cells and found that the mRNA expression of *Ccl2* was effectively suppressed (Fig. S20). ATS-9R-mediated silencing of *Ccl2* significantly reduced the levels of TNF- α , IL-6, IL-1 β and CCL2 in LPS-induced RAW264.7 cells, demonstrating that ATS-9R/siCcl2 complexes have an effective anti-inflammatory effect (Fig. 4G-J). The above data suggest that ATS-9R/siCcl2 complexes exert an anti-inflammatory effect in pro-inflammatory macrophages.

To confirm that the ATS-9R/siCcl2 complexes are accurately delivered to visceral adipose tissue, both Cy5.5-ATS-9R and Cy5.5-ATS-9R/siCcl2 complexes were injected intraperitoneally into GDM mice. The strong fluorescence intensities were most localized in VAT and SAT 8 h after injection and could be mostly cleared from SAT 24 h after injection (Fig. 5A and B, Fig. S21A), indicating targeted uptake of the ATS-9R/siCcl2 complexes into VAT.

A previous study has shown that ATS-9R specifically enters the epididymal adipose tissue and is preferentially internalized by macrophages [19]. To follow the intracellular transport of ATS-9R/siCcl2 complexes, BMDM cells were treated with Cy5.5-ATS-9R/siCcl2 complexes. The ATS-9R/siCcl2 complexes were well distributed in the cytoplasm after 4 h of incubation and in the nucleus after 48 h of incubation. (Fig. 5C). In addition, RAW264.7 cells took up ATS-9R/siCcl2 and reached a steady state after 24 h of incubation, and localization in

the nucleus was observed after 72 h of incubation (Fig. S22A). Similarly, ATS-9R can be internalized by BMDM cells and RAW264.7 cells (Fig. S21B and C).

It has been demonstrated that the uptake of ATS-9R in mouse ATMs is mediated by membrane prohibitin [23]. Prohibitin was expressed on the plasma membrane in BMDM cells and RAW264.7 cells (Fig. 5D and Fig. S22B). To verify the role of prohibitin in the internalization of ATS-9R/siCcl2 and the ability of ATS-9R/siCcl2 to target prohibitin, competition experiments were performed. BMDM cells and RAW264.7 cells were incubated simultaneously with or without Cy5.5-ATS-9R/siCcl2. The group incubated without ATS-9R/siCcl2 showed a significantly higher level of prohibitin than the group incubated with ATS-9R/siCcl2 (Fig. 5E-F and Fig. S22C-D). When the ATS-9R/siCcl2 complexes were internalized, the expression of prohibitin gradually decreased due to the binding of ATS-9R/siCcl2 to prohibitin, resulting in a continuous consumption of prohibitin. The Live Cell Imaging System vividly demonstrated the internalization of Cy5.5-ATS-9R/siCcl2 in RAW264.7 cells within 24 h (Supplementary video 1). Accordingly, ATS-9R binds to prohibitin located on the membrane of BMDM cells and RAW264.7 cells (Fig. S21D-G and Supplementary video 2). These observations demonstrate that ATS-9R/siCcl2 complexes target macrophages independent of differentiation status and are internalized into cells via a prohibitin-mediated mechanism.

3.5. ATS-9R/siCcl2 complexes alleviate inflammatory response through regulating Ca^{2+} and ROS signaling in ATMs

To validate the anti-inflammatory effect of the ATS-9R/siCcl2 complexes, the complexes were injected intraperitoneally into GDM mice (Fig. S23A). First, we analyzed the expression of inflammatory genes and found that the mRNA levels of *Tnf- α* , *Il-6*, *Il-1 β* , and *Ccl2* were reduced in ATMs of VAT from GDM mice treated with ATS-9R/siCcl2 complexes (Fig. S23B). Furthermore, administration of ATS-9R/siCcl2 complexes resulted in a reduction in the proportion of M1-phenotype macrophages and the ratio of M1/M2 macrophages, especially in VAT (Fig. 6). To further determine Ca^{2+} and ROS levels in ATMs from GDM mice with ATS-9R/siCcl2 complexes, flow cytometric analysis was performed, which showed that intracellular and mitochondrial Ca^{2+} and ROS levels were significantly reduced in ATMs, especially in visceral ATMs (Fig. 7). Taken together, these results suggest that targeting *Ccl2* silencing in ATMs by administration of ATS-9R/siCcl2 significantly attenuates the inflammatory response via blocking calcium transport between ER and mitochondria and reducing excessive ROS generation.

3.6. ATS-9R/siCcl2 complexes reduce blood cytokine levels and enhance insulin sensitivity

Although α CCL2 therapy showed significant inhibition of inflammatory factors in serum by inhibiting the expression of CCL2 in blood, targeting delivery of *Ccl2* siRNA to adipose tissue may be more effective in lowering blood glucose levels and improving insulin sensitivity in GDM mice. Therefore, we evaluated the therapeutic effect of ATS-9 R/siCcl2 complexes administered by four injections in late gestation. The main mechanisms proposed for GDM involve inflammatory cytokines in the bloodstream that are released from adipose tissue. To investigate the effect of ATS-9R/siCcl2 complexes on systemic inflammation in GDM mice, serum cytokine levels were analyzed. As shown in Fig. 8A-D, serum inflammatory cytokine levels were downregulated under ATS-9 R/siCcl2 complexes therapy, suggesting that suppression of adipose tissue inflammation affects overall inflammation. In addition, the OGTT and ITT results (Fig. 8E-H) showed that treatment with ATS-9R/siCcl2 complexes can effectively lower blood glucose levels and increase insulin sensitivity in GDM mice.

AKT is considered one of the most important signaling molecules for insulin to regulate liver, muscle and fat metabolism of glucose and lipids. Here, we found a decrease in p-AKT levels in the liver and muscle of HFD-induced GDM mice compared to the normal control group (Fig. S24A-B). In addition, we observed an increase of p-AKT levels in the liver and muscle of HFD mice treated with insulin compared to the HFD mice treated without insulin group (Fig. S24C-D), demonstrating the inactivation of AKT and the impaired insulin sensitivity in liver and muscle of HFD-induced GDM mice. Interestingly, treatment with the ATS-9R/siCcl2 complexes increased the expression of p-AKT (Fig. S24A-B), suggesting that the ATS-9R/siCcl2 complexes can improve insulin sensitivity in the liver and muscle of GDM mice.

Moreover, the reproductive outcome of GDM mice improved after treatment with ATS-9 R/siCcl2 (Fig. S25). Finally, systemic side effects are a major concern with gene-targeted therapy. As shown in Fig. S26, no obvious side effects or significant changes in liver and kidney function (ALT, AST and BUN) or routine blood tests (RBC, WBC and HGB) were observed before and after treatment with ATS-9 R/siCcl2 complexes. Taken together, the associations between ATS-9 R/siCcl2 accumulation in ATMs and attenuated IR indicate that CCL2 might be a promising therapeutic target for GDM pregnancies.

4. Discussion

Currently, there are various strategies to treat GDM, such as insulin and lifestyle interventions [24]. However, as obesity-induced inflammation is an important factor in the occurrence of GDM,

anti-inflammatory drugs targeting the systemic state of low-grade inflammation could be a potential therapeutic approach for GDM pregnancies. Although gene-mediated strategies to reduce obesity have been reported, they cannot be used in clinical trials because of their limited availability and inability to selectively target adipose tissue. In addition, long-term uncontrolled expression of therapeutic genes using viral vectors has shown serious side effects and even fatal consequences [25,26]. ATMs are potent targets for drug delivery due to their crucial role in obesity-related inflammation and metabolic disorders. *In vivo* studies have shown that ATS-9R has specificity for white adipose tissue and can bind to ATMs, leading to potential gene transfer to the SVF [19]. Based on this specific delivery system, we enclosed *Ccl2* siRNA with ATS-9R to create ATS-9R/siCcl2 complexes that could bind to prohibitin and were then successfully internalized into macrophages. These complexes were preferentially accumulated in ATMs by intraperitoneal injection and effectively alleviated obesity and systemic inflammation and consequently improved overall metabolism in GDM mice. Mechanistic studies showed that targeted delivery of *Ccl2* silencing into ATMs improved mitochondrial function by inhibiting excessive intracellular and mitochondrial Ca^{2+} and ROS production, thereby preventing ATMs from transitioning to the M1 pro-inflammatory phenotype.

Chronic inflammation of adipose tissue is an important etiologic mechanism associated with the increasing incidence of GDM [27]. Here, we demonstrated that the expression of pro-inflammatory factors is increased especially in the white VAT of GDM pregnancies. Excessive macrophage infiltration could lead to increased production of pro-inflammatory cytokines and mediators, which are the internal mechanism of inflammatory response, development, coordination and dissipation [28]. One of the aims of this study is to identify and validate potential targets for the treatment of GDM. RNA-seq analysis was performed on ATMs from normal and GDM pregnancies and KEGG analysis showed that the chemokine signaling pathway is significantly enriched in ATMs from GDM pregnancies. Chemokines are prime candidates for linking physiologic and pathologic pregnancy inflammation and for the pathogenesis of inflammatory crosstalk in GDM [14]. One of the interesting chemokines upregulated in ATMs of GDM pregnancies is CCL2. A recent meta-analysis showed a significant increase of the chemokine CCL2 in the serum of GDM patients [14]. CCL2 has been confirmed to have potential therapeutic effects [17], therefore CCL2 was selected as a research subject in this study.

Deficiency of *Ccl2* inhibits the expression of pro-inflammatory factors and the polarization of pro-inflammatory macrophages both *in vitro* and *in vivo*. Here we report that knockdown of *Ccl2* decreases the mRNA levels of *Tnf- α* , *Il-6* and *Il-1 β* , as well as the ratio of M1/M2 macrophages in LPS-induced RAW264.7 cells. In HFD-induced GDM mice, loss of *Ccl2* in ATMs also decreases the level of *Tnf- α* , *Il-6* and *Il-1 β* , inhibits the polarization of pro-inflammatory macrophages, and attenuates hyperglycemia and systemic inflammation. These results are consistent with the findings of Xinying Qi *et al.* who reported that CCL2 in serum was correlated with inflammatory cytokines, including IL-6 and TNF- α in GDM patients. Treatment of α CCL2 in C57 BL/KsJ^{db/+} mice attenuated GDM symptoms as well as the expression of inflammatory cytokines [16]. However, it is noteworthy that ATMs are composed of bone marrow-derived mononuclear macrophages (also known as recruitment macrophages) and adipose tissue resident macrophages. Nehemiah Cox *et al.* have shown that adipose tissue resident macrophages are the "culprits" that lead to obesity [29]. Furthermore, adipose tissue-resident macrophages play an important role in the progression of adipose tissue inflammation, and CCL2 can promote the proliferation of these resident macrophages *in situ* [30]. CCL2 is also known to be involved in the recruitment of mononuclear macrophages [31]. Therefore, ATS-9R/siCcl2 complexes *in vivo* may simultaneously reduce excessive adipose tissue-resident macrophages and inhibit monocytes recruitment, thereby alleviating local and systemic inflammation, warranting further investigation. In addition, inhibition of CCR2-dependent macrophage recruitment can prevent obesity-induced adipose tissue

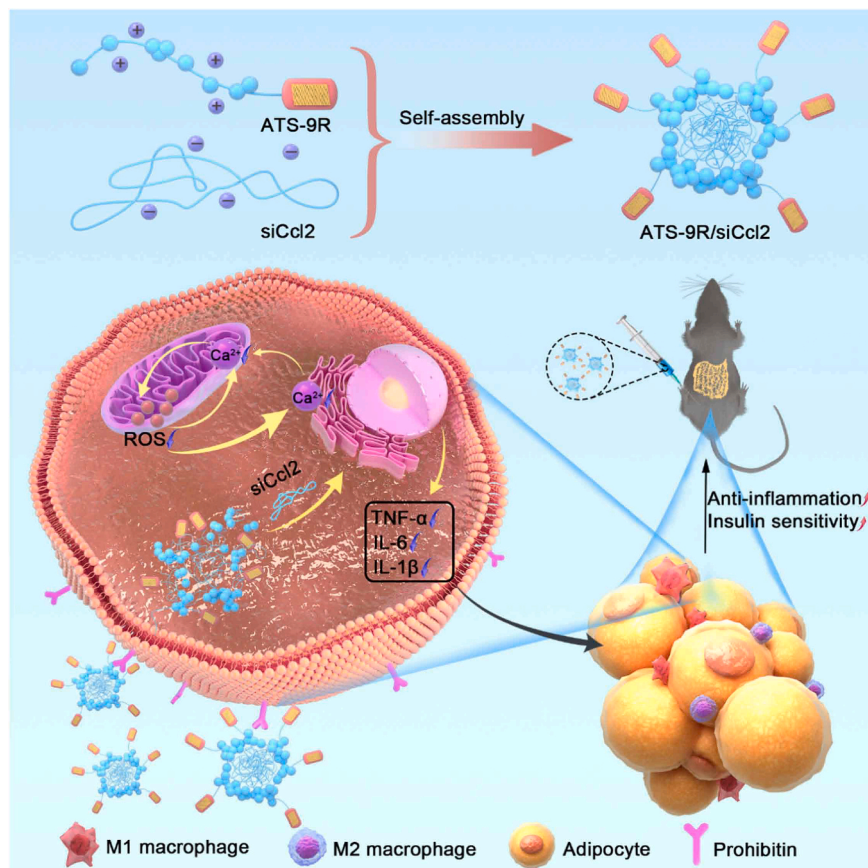


Fig. 9. A schematic illustration showing how the ATS-9R/siCcl2 oligopeptide complexes targeting adipose tissue attenuate insulin resistance in GDM. In women with GDM, the level of CCL2 is elevated in ATMs. ATS-9R/siCcl2 complexes can preferentially accumulate in the adipose tissue and selectively target pro-inflammatory ATMs via the cell membrane protein prohibitin, releasing *Ccl2* siRNA. *Ccl2* silencing in ATMs blocks calcium transport between ER and mitochondria and reduces excessive ROS generation, further mitigating local and systemic inflammatory response and improving insulin sensitivity.

inflammation, IR and metabolic syndrome, but has no effect on adipocyte size and weight [29]. Thus, in GDM mice, ATS-9R/siCcl2 complexes may play a role mainly in pro-inflammatory macrophages rather than adipocytes.

In this study, we found that CCL2 plays a crucial role in the regulation of Ca^{2+} transport in macrophages. Research has shown that chemokine signaling alters intracellular Ca^{2+} dynamics in many cell types [32]. Silencing of *Ccl2* reduced intracellular and mitochondrial Ca^{2+} levels in both LPS-stimulated RAW264.7 cells and ATMs from GDM mice. The interactions between ROS and Ca^{2+} signaling can be considered bidirectional, and a reduction in mitochondrial calcium uptake is an important factor in alleviating inflammation [33,34]. Increasing mitochondrial Ca^{2+} levels can generate ROS, which can then diffuse out of the mitochondria and target ER Ca^{2+} channels, resulting in the release of Ca^{2+} that amplifies ROS signaling and further impairs mitochondrial function and energy metabolism [35–37]. It has also been found that the length of MAM increases in LPS-stimulated macrophages with *Ccl2* deficiency, and this elongation is unfavorable for excessive calcium transfer from the ER to mitochondria [36,37]. These results demonstrate that CCL2 plays a critical role in the inflammatory response of macrophages by blocking calcium transport from the ER to the mitochondria and reducing excessive ROS generation. However, it should be noted that Fendiline and MitoQ attenuate the inflammatory response in macrophages, suggesting that Ca^{2+} and ROS signaling may not be the direct requirement for CCL2 function.

5. Conclusion

In summary, the present study reveals that CCL2 is enriched in the

ATMs of GDM patients and that targeted administration of ATS-9R/siCcl2 complexes into adipose tissue could suppress pro-inflammatory macrophage activation and attenuate metabolic disorders in HFD-induced GDM mice by *Ccl2* silencing to block calcium transport between ER and mitochondria and reduce excessive ROS production (Fig. 9). Targeting the ATS-9R/siCCL2 complexes to adipose tissue represents a promising therapeutic strategy for future GDM pregnancies.

CRedit authorship contribution statement

Min Wang: Writing – original draft, Validation, Methodology, Data curation, Conceptualization. **Xuyang Chen:** Validation, Formal analysis. **Xiaobo Zhou:** Writing – review & editing, Supervision. **Hua Zhang:** Writing – review & editing, Supervision, Project administration, Funding acquisition, Conceptualization. **Dan Zhang:** Methodology, Data curation. **Bailong Tao:** Methodology, Data curation. **Linwei Zhou:** Methodology, Data curation. **Hongli Li:** Visualization, Data curation. **Bingnan Chen:** Investigation, Formal analysis. **Hao Chen:** Investigation, Formal analysis. **Yanshan Shang:** Validation, Formal analysis.

Declaration of Competing Interest

The authors declare that they have no known competing financial interests or personal relationships that could have appeared to influence the work reported in this paper

Data availability

Data will be made available on request.

Acknowledgments

This study was supported by the National Natural Science Foundation of China (No. 81971406, 82271715), The 111 Project (Yuwaizhuan (2016)32), China Postdoctoral Science Foundation (No. 2023M740453), Chongqing Science & Technology Commission (cstc2021jcyj-msxmX0213), Natural Science Foundation of Chongqing, China (CSTB2022NSCQ-MSX1679), Chongqing Municipal Education Commission (KJZD-K202100407), Chongqing Health Commission and Chongqing Science & Technology Commission (2021MSXM121).

Appendix A. Supporting information

Supplementary data associated with this article can be found in the online version at [doi:10.1016/j.biopha.2024.116775](https://doi.org/10.1016/j.biopha.2024.116775).

References

- [1] E.D. Szmulowicz, J.L. Josefson, B.E. Metzger, Gestational diabetes mellitus, *Endocrinol. Metab. Clin. North Am.* 48 (3) (2019) 479–493, <https://doi.org/10.1016/j.ecl.2019.05.001>.
- [2] A. Sweeting, J. Wong, H.R. Murphy, G.P. Ross, A clinical update on gestational diabetes mellitus, *Endocr. Rev.* 43 (5) (2022) 763–793, <https://doi.org/10.1210/edrv/bnac003>.
- [3] E.C. Johns, F.C. Denison, J.E. Norman, R.M. Reynolds, Gestational diabetes mellitus: mechanisms, treatment, and complications, *Trends Endocrinol. Metab.* 29 (11) (2018) 743–754, <https://doi.org/10.1016/j.tem.2018.09.004>.
- [4] P. El Meouchy, M. Wahoud, S. Allam, R. Chedid, W. Karam, S. Karam, Hypertension related to obesity: pathogenesis, characteristics and factors for control, *Int. J. Mol. Sci.* 23 (20) (2022) 12305, <https://doi.org/10.3390/ijms232012305>.
- [5] C.J. McElwain, F.P. McCarthy, C.M. McCarthy, Gestational diabetes mellitus and maternal immune dysregulation: what we know so far, *Int. J. Mol. Sci.* 22 (8) (2021) 4261, <https://doi.org/10.3390/ijms22084261>.
- [6] K.E. Skórzyńska-Dziduszko, Ż. Kimber-Trojnar, J. Patro-Malyszka, A. Olszewska, T. Zaborowski, T. Malecka-Massalska, An interplay between obesity and inflammation in gestational diabetes mellitus, *Curr. Pharm. Biotechnol.* 17 (7) (2016) 603–613, <https://doi.org/10.2174/1389201017666160127105926>.
- [7] H. Li, Y. Meng, S. He, X. Tan, Y. Zhang, X. Zhang, L. Wang, W. Zheng, Macrophages, chronic inflammation, and insulin resistance, *Cells* 11 (19) (2022) 3001, <https://doi.org/10.3390/cells11193001>.
- [8] Y. Dong, M. Chauhan, A. Betancourt, M. Belfort, C. Yallampalli, Adipose tissue inflammation and adrenomedullin overexpression contribute to lipid dysregulation in diabetic pregnancies, *J. Clin. Endocrinol. Metab.* 103 (10) (2018) 3810–3818, <https://doi.org/10.1210/jc.2018-00905>.
- [9] S. Zhu, M. Liu, S. Bennett, Z. Wang, K.D.G. Pfeleger, J. Xu, The molecular structure and role of CCL2 (MCP-1) and C-C chemokine receptor CCR2 in skeletal biology and diseases, *J. Cell. Physiol.* 236 (10) (2021) 7211–7222, <https://doi.org/10.1002/jcp.30375>.
- [10] M.K. Georgakakis, J. Bernhagen, L.H. Heitman, C. Weber, M. Dichgans, Targeting the CCL2-CCR2 axis for atheroprotection, *Eur. Heart J.* 43 (19) (2022) 1799–1808, <https://doi.org/10.1093/eurheartj/ehac094>.
- [11] T. Yoshimura, C. Li, Y. Wang, A. Matsukawa, The chemokine monocyte chemoattractant protein-1/CCL2 is a promoter of breast cancer metastasis, *Cell. Mol. Immunol.* 20 (7) (2023) 714–738, <https://doi.org/10.1038/s41423-023-01013-0>.
- [12] M. Ooms, A. Strom, K. Strassburger, B. Menart, R.D. Leslie, N.C. Schloot, Increased spontaneous CCL2 (MCP-1) and CCL5 (RANTES) secretion in vitro in LADA compared to type 1 diabetes and type 2 diabetes: action LADA 14, *Diabetes/Metab. Res. Rev.* 37 (7) (2021) e3431, <https://doi.org/10.1002/dmrr.3431>.
- [13] J. Huber, F.W. Kiefer, M. Zeyda, B. Ludvik, G.R. Silberhumer, G. Prager, G. J. Zlabinger, T.M. Stulnig, CC chemokine and CC chemokine receptor profiles in visceral and subcutaneous adipose tissue are altered in human obesity, *J. Clin. Endocrinol. Metab.* 93 (8) (2008) 3215–3221, <https://doi.org/10.1210/jc.2007-2630>.
- [14] H. Liu, A. Liu, A.C. Kaminga, J. McDonald, S.W. Wen, X. Pan, Chemokines in gestational diabetes mellitus, *Front. Immunol.* 13 (2022) 705852, <https://doi.org/10.3389/fimmu.2022.705852>.
- [15] S. Dommel, M. Blüher, Does C-C Motif Chemokine Ligand 2 (CCL2) Link Obesity to a Pro-Inflammatory State? *Int. J. Mol. Sci.* 22 (3) (2021) 1500, <https://doi.org/10.3390/ijms22031500>.
- [16] X. Qi, Y. Xing, X. Wang, Blockade of CCL2/CCR2 signaling pathway exerts anti-inflammatory effects and attenuates gestational diabetes mellitus in a genetic mice model, *Horm. Metab. Res. = Horm. - und Stoffwechs. = Horm. Et. Metab.* 53 (1) (2021) 56–62, <https://doi.org/10.1055/a-1250-8221>.
- [17] Z. Cai, X. Wu, Z. Song, S. Sun, Y. Su, T. Wang, X. Cheng, Y. Yu, C. Yu, E. Chen, W. Chen, Y. Yu, A. Linkermann, J. Min, F. Wang, Metformin potentiates nephrotoxicity by promoting NETosis in response to renal ferroptosis, *Cell Discov.* 9 (1) (2023) 104, <https://doi.org/10.1038/s41421-023-00595-3>.
- [18] K.A. Boggess, A. Valint, J.S. Refuerzo, N. Zork, A.N. Battarbee, K. Eichelberger, G. A. Ramos, G. Olson, C. Durnwald, M.B. Landon, K.M. Aagaard, K. Wallace, C. Scifres, T. Rosen, W. Mulla, A. Valent, S. Longo, L. Young, M.A. Marquis, S. Thomas, D. Berry, Metformin plus insulin for preexisting diabetes or gestational diabetes in early pregnancy: the MOMPOD randomized clinical trial, *JAMA* 330 (22) (2023) 2182–2190, <https://doi.org/10.1001/jama.2023.22949>.
- [19] S.B. Yong, Y. Song, Y.H. Kim, Visceral adipose tissue macrophage-targeted TACE silencing to treat obesity-induced type 2 diabetes, *Biomaterials* 148 (2017) 81–89, <https://doi.org/10.1016/j.biomaterials.2017.09.023>.
- [20] J.V. Cabral-Costa, A.J. Kowaltowski, Mitochondrial Ca²⁺ handling as a cell signaling hub: lessons from astrocyte function, *Essays Biochem.* 67 (1) (2023) 63–75, <https://doi.org/10.1042/EBC20220094>.
- [21] S. Patergnani, J.M. Suski, C. Agnoletto, A. Bononi, M. Bonora, E. De Marchi, C. Giorgi, S. Marchi, S. Missiroli, F. Poletti, A. Rimessi, J. Duszynski, M. R. Wieckowski, P. Pinton, Calcium signaling around Mitochondria Associated Membranes (MAMs), *Cell Commun. Signal.* 9 (2011) 19, <https://doi.org/10.1186/1478-811X-9-19>.
- [22] T.M. Bauer, E. Murphy, Role of mitochondrial calcium and the permeability transition pore in regulating cell death, *Circ. Res.* 126 (2) (2020) 280–293, <https://doi.org/10.1161/CIRCRESAHA.119.316306>.
- [23] A. Homayouni, N. Bagheri, S. Mohammad-Alizadeh-Charandabi, N. Kashani, N. Mobaraki-Asl, M. Mirghafurvand, H. Asgharian, F. Ansari, H. Pourjafar, Prevention of Gestational Diabetes Mellitus (GDM) and probiotics: mechanism of action: a review, *Curr. Diabetes Rev.* 16 (6) (2020) 538–545, <https://doi.org/10.2174/1573399815666190712193828>.
- [24] J.F. Plows, J.L. Stanley, P.N. Baker, C.M. Reynolds, M.H. Vickers, The pathophysiology of gestational diabetes mellitus, *Int. J. Mol. Sci.* 19 (11) (2018) 3342, <https://doi.org/10.3390/ijms19113342>.
- [25] L. Cao, E.J. Lin, M.C. Cahill, C. Wang, X. Liu, M.J. Doring, Molecular therapy of obesity and diabetes by a physiological autoregulatory approach, *Nat. Med.* 15 (4) (2009) 447–454, <https://doi.org/10.1038/nm.1933>.
- [26] H. Dhillon, S.P. Kalra, V. Prima, S. Zolotukhin, P.J. Scarpace, L.L. Moldawer, N. Muzyczka, P.S. Kalra, Central leptin gene therapy suppresses body weight gain, adiposity and serum insulin without affecting food consumption in normal rats: a long-term study, *Regul. Pept.* 99 (2–3) (2001) 69–77, [https://doi.org/10.1016/S0167-0115\(01\)00237-3](https://doi.org/10.1016/S0167-0115(01)00237-3).
- [27] T. Lekva, E.R. Norwitz, P. Aukrust, T. Ueland, Impact of systemic inflammation on the progression of gestational diabetes mellitus, *Curr. Diabetes Rep.* 16 (4) (2016) 26, <https://doi.org/10.1007/s11892-016-0715-9>.
- [28] A. Harlev, B. Aricha-Tamir, R. Shaco-Levy, T. Tarnovskii, N. Bashan, A. Rudich, E. Sheiner, F. Press, A. Wiznitzer, Macrophage infiltration and stress-signaling in omental and subcutaneous adipose tissue in diabetic pregnancies, *J. Matern. -Fetal Neonatal Med.* 27 (12) (2014) 1189–1194, <https://doi.org/10.3109/14767058.2013.853734>.
- [29] N. Cox, L. Crozet, I.R. Holtman, P.L. Loyher, T. Lazarov, J.B. White, E. Mass, E. R. Stanley, O. Elemento, C.K. Glass, F. Geissmann, Diet-regulated production of PDGF α by macrophages controls energy storage, *Science (New York, N.Y.)* 373 (6550) (2021) eabe9383, <https://doi.org/10.1126/science.abe9383>.
- [30] S.U. Amano, J.L. Cohen, P. Vangala, M. Tencerova, S.M. Nicoloso, J.C. Yawe, Y. Shen, M.P. Czech, M. Aouadi, Local proliferation of macrophages contributes to obesity-associated adipose tissue inflammation, *Cell Metab.* 19 (1) (2014) 162–171, <https://doi.org/10.1016/j.cmet.2013.11.017>.
- [31] M. Xu, Y. Wang, R. Xia, Y. Wei, X. Wei, Role of the CCL2-CCR2 signalling axis in cancer: Mechanisms and therapeutic targeting, *Cell Prolif.* 54 (10) (2021) e13115, <https://doi.org/10.1111/cpr.13115>.
- [32] A.F. Alharbi, J. Parrington, Deciphering the role of endolysosomal Ca²⁺ channels in immunity, *Front. Immunol.* 12 (2021) 656965, <https://doi.org/10.3389/fimmu.2021.656965>.
- [33] J.C. McNelis, J.M. Olefsky, Macrophages, immunity, and metabolic disease, *Immunity* 41 (1) (2014) 36–48, <https://doi.org/10.1016/j.immuni.2014.05.010>.
- [34] A. Görlach, K. Bertram, S. Hudecova, O. Krizanova, Calcium and ROS: a mutual interplay, *Redox Biol.* 6 (2015) 260–271, <https://doi.org/10.1016/j.redox.2015.08.010>.
- [35] G. Ciccarelli, S. Conte, G. Cimmino, P. Maiorano, A. Morrione, A. Giordano, Mitochondrial dysfunction: the hidden player in the pathogenesis of atherosclerosis? *Int. J. Mol. Sci.* 24 (2) (2023) 1086, <https://doi.org/10.3390/ijms24021086>.
- [36] A. Rossi, P. Pizzo, R. Filadi, Calcium, mitochondria and cell metabolism: a functional triangle in bioenergetics, *Biochim. Biophys. Acta Mol. Cell Res.* 1866 (7) (2019) 1068–1078, <https://doi.org/10.1016/j.bbamcr.2018.10.016>.
- [37] H. Mao, W. Chen, L. Chen, L. Li, Potential role of mitochondria-associated endoplasmic reticulum membrane proteins in diseases, *Biochem. Pharmacol.* 199 (2022) 115011, <https://doi.org/10.1016/j.bcp.2022.115011>.